Second-harmonic generation in one-dimensional photonic edge waveguides

Y. Dumeige, F. Raineri, and A. Levenson
Laboratoire de Photonique et de Nanostructures (CNRS UPR 20), Route de Nozay, 91460 Marcoussis, France

X. Letartre
Laboratoire d'Electronique Optoélectronique et Microsystèmes (CNRS UMR 5512), 36, Avenue Guy de Collongue, 69134 Ecully Cedex, France

(Received 23 April 2003; published 31 December 2003)

Diffraction losses in one-dimensional photonic crystal (PC) waveguides are the primary limitation on second-harmonic (SH) conversion efficiency. By using a finite difference time domain (FDTD) code taking into account second-order nonlinear polarization, we investigated these losses numerically, particularly at the SH wavelength. We propose an efficient SH conversion scheme in $Al_xGa_{1-x}As$/air-etched waveguides. An analytical model is used to extrapolate the conversion efficiency to a number of periods for which time consumption makes the FDTD codes unsuitable.

DOI: 10.1103/PhysRevE.68.066617 PACS number(s): 42.65.Wi, 42.65.Ky, 42.70.Nq

I. INTRODUCTION

The use of dispersive properties of stratified media was proposed very early in the history of nonlinear optics as a means of either phase-matched or enhanced second-order nonlinear interactions [1,2]. More recently, two important breakthroughs have renewed the interest in nonlinear stratified media. First, analytical and numerical approaches are now able to describe second-order nonlinear interactions in finite stratified media [3,4]; second, there has been tremendous evolution in micro- and nanotechnologies. They are now able to produce structures with a one- (1D) or two-dimensional (2D) periodicity smaller than the nonlinearly interacting wavelengths [5]. For instance, in a recent paper we experimentally demonstrated that it is possible to achieve phase matching and field enhancement simultaneously by engineering the dispersive properties of a 1D-periodic stratified medium composed of a low refractive index linear material and a high-index nonlinear material [6]. These combined effects were exploited to achieve a second-harmonic external conversion efficiency of 0.1% with a fundamental field (FF) pulse peak power of 8 kW incident on a structure constituted of 18 periods of $Al_xGa_{1-x}As/AlO_x$ (respectively the nonlinear and linear layers). Its total length is as short as 4.9 μm. Moreover, by comparing the results obtained for several equivalent structures having different numbers of unit cells, the second-harmonic efficiency was demonstrated to grow faster than the fifth power of the structure length. This dependence of second-harmonic generation (SHG) efficiency, now well understood theoretically [7], is far better than the usual quadratic behavior associated with second-order nonlinear process and opens the way to ultrashort wavelength converters.

In this context, it is of primary interest to consider the possibility of combining the above mentioned advantages associated with nonlinear periodic stratified structures and those associated with a waveguided operation. Waveguiding, in 1D or 2D structures, offers indeed a twofold advantage: it allows a supplementary field enhancement due to transverse field confinement and it avoids problems associated with the eventual spatial walk-off between the interacting fields due to non-null incident angle. In $Al_xGa_{1-x}As$ waveguides (WGs) it also allows one to benefit from the highest value of the quadratic nonlinear tensor [8]. Nevertheless, guided operation introduces new drawbacks associated, in particular, with the need to achieve guiding at two very distant wavelengths such as those of the FF and the SH. Also, the use of stratified media, with a high contrast of indices between the linear and nonlinear layers, could induce an additional source of losses, particularly at SH wavelength. These intuitive arguments show that special care should be taken in the optimization of the field confinement at second-harmonic wavelength, in order to avoid or minimize radiative losses [9]. This is particularly true in the case where the second-harmonic frequency is above the light cone and is easily coupled to radiative modes [10]. The problem of modes above the light cone was recently addressed in detail in the linear regime by Lalanne [11], but its consequences in the nonlinear regime have been neglected in the literature so far.

In this paper, we transpose the ideas previously demonstrated in vertical structures to a 1D-periodic air/$Al_xGa_{1-x}As$ waveguide able to phase-match the nonlinear interaction and to enhance both the FF and SH. A nonlinear 2D finite difference time domain (NL FDTD) code is used to predict the SHG efficiency in such a structure. The role of losses at the SH frequency is discussed for different waveguide thicknesses. More than 5% SHG conversion efficiency is predicted for an optimized 5-μm-long structure excited by a FF with a peak power of 600 W. We finish the discussion of the potential of the considered structure by introducing an analytical model that considers the segmented waveguide as a doubly resonant cavity.

II. NONLINEAR 1D-PC WAVEGUIDE STRUCTURE AND LINEAR PROPERTIES

A schematic view of a typical NL 1D-PC WG structure is represented in Fig. 1. The structure could be obtained by epitaxial growth on a GaAs [001]–oriented substrate. It is composed of an *N*-periods Bragg grating oriented

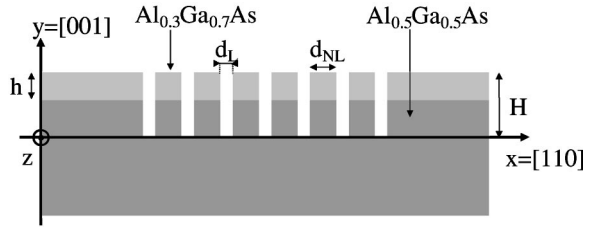

FIG. 1. Structure parameters. [001] corresponds to the *y* axis and [110] to the *x* axis. d_L and d_{NL} are, respectively, the lengths of the linear and the nonlinear layers. $Al_{0.3}Ga_{0.7}As$ and $Al_{0.5}Ga_{0.5}As$ are represented in light and dark gray.

along the [110] crystallographic axis deeply etched in an $Al_xGa_{1-x}As$ planar waveguide. The waveguide is composed of a substrate of $Al_{0.5}Ga_{0.5}As$, a nonlinear layer of $Al_{0.3}Ga_{0.7}As$ with a nonlinear effective susceptibility of $d_{14}=120$ pm/V around 1.55 μm, and air; in the *z* direction the refractive index is homogeneous. The Λ-periodic Bragg grating features are d_{NL} and d_L, respectively, the length of the nonlinear material and the length of the air gaps. The $Al_{0.3}Ga_{0.7}As$ layer thickness and air-gap depth are *h* and *H*. Evidently, as is the case in bulk 1D-periodic structures, the linear and nonlinear behavior of the NL 1D-PC WG strongly depend on d_{NL} and d_L. In the case of WG operation, they also depend on the *h* and *H* values, which determine the transverse field confinement and diffraction.

As in our previous work in planar Bragg structures [6], we design the NL 1D-PC WG so as to have the FF resonant with the first transmission peak on the right side (in wavelength) of the first-order band gap. This choice is not arbitrary since it allows an important FF enhancement. In turn, it imposes the spectral position of the SH. Indeed, the Bloch phase accumulated by the FF is $(\pi/N)(N-1)$. In order to ensure phase matching, the SH should escape the structure at the second transmission peak on the right side of the second-order band gap. At this peak the accumulated Bloch phase is $(\pi/N)(2N-2)$, exactly the one needed for phase matching [4]. In the following the NL 1D-PCs are designed under such conditions for a FF polarized parallel to the *z* direction (see Fig. 1) and a SH polarized in the [*x*,*y*] plane. These polarizations allow exploiting the maximum value of the second-order nonlinear tensor. Note that by changing the number of periods and/or *h* and *H*, the conditions of the double resonance are modified. In order to avoid any misalignment of the double resonance and to keep the nonlinear material thickness constant, we force the value of the index of refraction of the nonlinear material ($Al_{0.3}Ga_{0.7}As$) at SH in the calculations.

We use a FDTD [12] code to analyze the linear properties of the NL 1D-PC structures. We first consider a structure defined by $d_{\mathrm{NL}}=150$ nm, $d_L=95$ nm, $h=1$ μm, and $H=1.8$ μm. Note that the waveguide supports two modes at FF wavelength and three at SH wavelength. In Fig. 2 are represented reflection and transmission linear spectra for the first mode around the FF [Fig. 2(a)] and the SH [Fig. 2(b)] wavelengths, indicated by the arrows. The number of periods is $N=8$. Figures 2(a) and 2(b) clearly show the usual photonic band gaps (PBGs) and lateral transmission peaks. It also

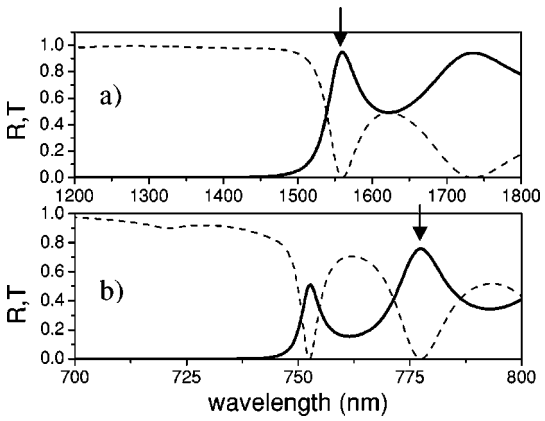

FIG. 2. Coefficients of transmission (*T*) (solid line) and reflection (*R*) (dashed line) of the eight-period $h=1$ μm structure around the FF wavelength (a) and the SH wavelength (b).

appears that the stop bands are not totally flat and the reflection peak does not attain a value of unity. These features are more pronounced at the SH wavelength and essentially attest the detrimental role played by losses. As the number of periods increases the transmission peaks become sharper as illustrated, around the SH wavelength, in Fig. 3 for $N=10$, 12, 15, and 20. At the same time the transmission and reflection peaks start to vanish and the first transmission peak at the right side of the PBG edge almost disappears when $N=20$.

These effects are essentially due to diffraction losses in air at frequencies situated above the light cone (in our case, the etching depth is sufficient to prevent leakage toward the $Al_{0.5}Ga_{0.5}As$ substrate). One can also remark that the peaks close to the PBG edge are principally affected. This effect can be understood as follows. To each transmission peak is associated an increase of the density of optical modes (DOMs) with respect to that of a homogeneous medium having equivalent macroscopic constants [13]. This increase of photon lifetime at transmission peaks could be viewed as an effect of the resonator distributed over the whole Bragg structure. The sharpness of transmission peaks situated close

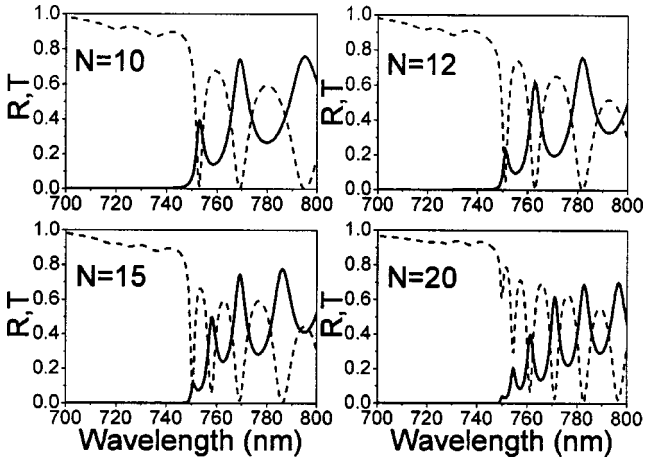

FIG. 3. Coefficients of transmission (*T*) (solid line) and reflection (*R*) (dashed line) of the 10-, 12-, 15-, and 20-period $h=1$ μm structures around the SH wavelength.

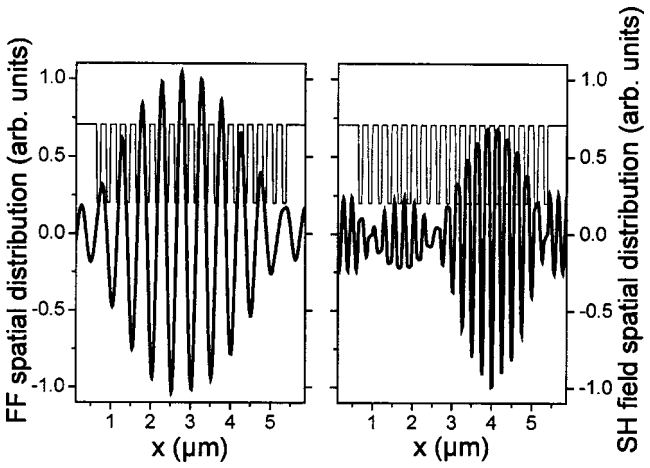

FIG. 4. Spatial field distribution at FF and SH phase-matched wavelengths in the 20-period $h=1\ \mu$m structure. The thick line represents the spatial distribution and the thin line the refractive index.

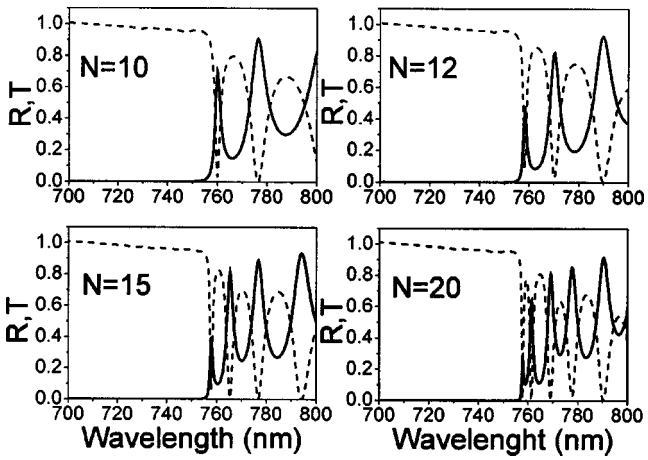

FIG. 5. Coefficients of transmission (T) (solid line) and reflection (R) (dashed line) of the 10-, 12-, 15-, and 20-period $h=2\ \mu$m structures around the SH wavelength.

to the PBG edge reveals, at these wavelengths, a high equivalent Q factor of the distributed resonator. This means that the number of semiconductor/air interfaces to which the SH is sensitive is substantially increased by the number of round trips in the distributed resonator. As a consequence the SH losses grow with the Q factor. We will come back to the cavity analogy in the last section.

We have represented in Fig. 4 the spatial field profile at the FF (first transmission peak at the right side of the first PBG edge) and SH (second transmission peak at the right side of the second PBG edge) wavelengths for the 20-period structure. The FF presents the expected symmetric localized behavior. The SH is expected to have two equivalent symmetric lobes, whereas Fig. 4 clearly shows a spatial distribution highly distorted by the presence of losses. This is essentially due to a strong coupling with a dissipative reservoir that breaks the symmetry of the system.

As we will show later on, diffraction losses and their effect of washing out the transmission resonances and distorting the SH are extremely detrimental to SHG efficiency. The losses are essentially governed by three factors having a combined effect: mode size, energy with respect to the light cone, and filling factor. Different avenues are offered in order to diminish diffraction losses at the SH wavelength. Among them, mode size enlargement appears as the most direct solution compatible with the constraints imposed by phase matching and FF and SH field enhancement. Indeed, here phase matching is obtained for a SH frequency located above the light cone. A possible way to enlarge the mode size is to increase the WG thickness.

In the following we consider the effect of the increase of WG thickness. Keeping in mind the aim of an experimental implementation of the approach we have chosen $H=3\ \mu$m for the air-gap depths. These values are compatible with state of the art technology in $Al_xGa_{1-x}As$ compounds. In Fig. 5 are represented for $N=10$, 12, 15, and 20, the calculated reflection and transmission linear spectra around the SH wavelength (first mode) for $h=2\ \mu$m, $d_{NL}=150$ nm, and $d_L=95$ nm. Note that the waveguide still supports two modes at FF wavelength, but five at SH wavelength. In contrast to Fig. 3, flat stop bands and well defined transmission and reflection resonances are still observed for $N=15$ and 20, demonstrating the diminution of losses as the mode size is increased. Note that, in the simulations, the input field is a short pulse whose spectral extension allows one to calculate the linear scattering properties of the structure over a wide range of wavelengths. In Fig. 5, the central wavelength of the pulse is 775 nm. Far from this value, the field amplitude might be too small to maintain the numerical accuracy. This is the case around 700 nm where the normalized reflectivity spectrum is greater than unity. We represented in Fig. 6 the spatial field distribution obtained at FF and SH wavelengths. In the present case, both FF and SH profiles are close to those optimizing the overlap between their product and the nonlinear susceptibility [3,7]. We stress that losses at SH frequency are not related to a mode conversion but come from the transverse extension of the mode.

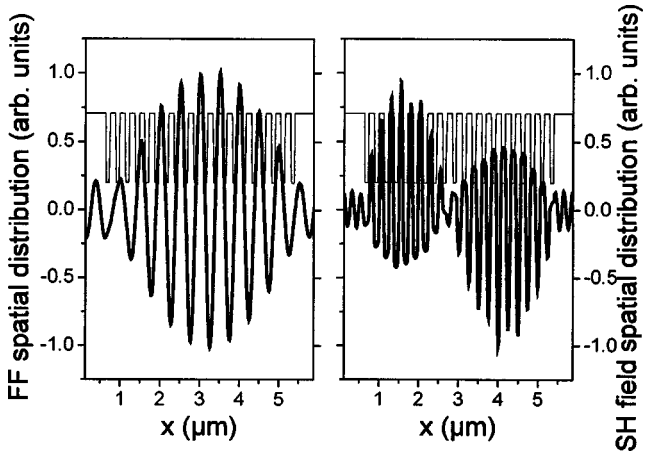

FIG. 6. Spatial field distribution at FF and SH phase-matched wavelengths of the 20-period $h=2\ \mu$m structure. The thick line represents the spatial distribution and the thin line the refractive index.

III. NONLINEAR OPERATION OF 1D PCS

As in the linear case, a nonlinear 2D FDTD code seems to be the more complete way to describe SHG in structures such as the 1D-PC waveguides. 2D FDTD was only recently extended to include second-order nonlinear interactions in 2D structures by Shi *et al.* [14]. In Ref. [14] the second-order nonlinear interaction is considered in the presence of FF depletion and cascaded second-order nonlinearity. The chromatic dispersion is taken into account recursively. This method is thus of general interest at the price of time-consuming codes well adapted to analyze SHG in realistic 1D or 2D structures, periodical or not. Nevertheless, it is hardly able to attack the difficult and time-consuming problem of optimization of the geometrical parameters; in addition, it applies only to a scalar interaction.

We recently developed a NL FDTD method that is able to deal with a vectorial nonlinear interaction and presents a reasonable computational time at the expense of loosing generality. In particular, the method works in the nondepleted pump approximation and neglects intrapulse chromatic dispersion [15]. It is based on the implementation of two parallel linear FDTD codes, the first operating at FF wavelength and the second at SH wavelength. The quadratic nonlinearity is taken into account only for the SH, which is not coupled back to the FF wavelength. Chromatic dispersion is considered simply by taken the actual refractive index at FF and SH wavelengths. This artificial separation of FF and SH propagation allows one to easily identify FF and SH distributions.

In the particular case considered here, due to the second-order susceptibility tensor of $Al_xGa_{1-x}As$, following the Yee algorithm [12] the equation of SH evolution reads

$$H^{\mathrm{SH},n+1/2}_{z,i+1/2,j+1/2}=H^{\mathrm{SH},n-1/2}_{z,i+1/2,j+1/2}+\frac{\Delta t}{\mu_0\Delta}(E^{\mathrm{SH},n}_{y,i,j+1/2}-E^{\mathrm{SH},n}_{y,i+1,j+1/2}+E^{\mathrm{SH},n}_{x,i+1/2,j+1}-E^{\mathrm{SH},n}_{x,i+1/2,j}), \tag{1a}$$

$$E^{\mathrm{SH},n+1}_{x,i+1/2,j}=E^{\mathrm{SH},n}_{x,i+1/2,j}+\frac{\Delta t}{\varepsilon^{\mathrm{SH}}_{i,j}\Delta}(H^{\mathrm{SH},n+1/2}_{z,i+1/2,j+1/2}-H^{\mathrm{SH},n+1/2}_{z,i+1/2,j-1/2}), \tag{1b}$$

$$E^{\mathrm{SH},n+1}_{y,i,j+1/2}=E^{\mathrm{SH},n}_{y,i+1/2,j}+\frac{\Delta t}{\varepsilon^{\mathrm{SH}}_{ij}\Delta}(H^{\mathrm{SH},n+1/2}_{z,i-1/2,j+1/2}-H^{\mathrm{SH},n+1/2}_{z,i+1/2,j+1/2})\frac{1}{\varepsilon^{\mathrm{SH}}_{i,j}}(P^{(2)n+1/2}_{y,i,j+1/2}-P^{(2),n-1/2}_{y,i,j+1/2}), \tag{1c}$$

where x, y, and z are defined in Fig. 1, Δ is the spatial step, $\Delta t=\Delta/2c$ is the temporal step ($\Delta=12.5$ nm in all our simulations), and $\varepsilon^{\mathrm{SH}}_{ij}$ is the dielectric constant at (i,j) for the SH. Note that this numerical method could be improved using two different computation grids and steps for the FF and SH. In this case, the total computation time and the memory usage could be decreased by a factor of 2. In expression (1c) the third term on the right side is the non-null component of the nonlinear polarization $\mathbf{P}^{(2)}=\hat{\mathbf{y}}\varepsilon_0 d_{14}(E^{\mathrm{FF}}_z)^2$, where E^{FF}_z is the electric field polarized along the z direction at FF frequency, evaluated via the usual FDTD method.

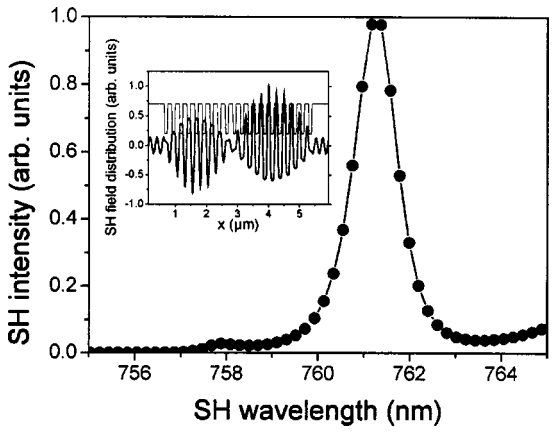

FIG. 7. Transmission spectrum of the generated SH in the 20-period $h=2\ \mu$m structure. Inset: Spatial field distribution of the generated SH. The thick line represents the spatial distribution and the thin line the refractive index.

In Fig. 7 is represented, for the optimized structure ($h=2\ \mu$m, 20 periods), the normalized spectrum of the SH generated. The input FF pulse duration is 75 fs, corresponding to a full width at half maximum spectrum of 45 nm. The use of such a short pulse is a practical way to obtain, after the proper quadratic normalization by the FF envelope, an equivalent of the phase-matching curve without varying the FF central wavelength. Two peaks clearly appear (at 757.9 and 761.4 nm); they correspond to the first two transmission resonances at the right side of the second PBG edge. The highest SHG is obtained at the 761.4 nm peak, the one that ensures phase matching. At this wavelength the generated SH field distribution, represented in the inset of Fig. 7, follows that of the linear field at the same frequency (see Fig. 6). Note that an intense third peak, not represented in the figure, also appears at the wavelength of the third lateral resonance. The relative value of these three peaks in the pulsed regime depends on the density of modes, phase matching, spectral filtering, and group velocity mismatch [16]. We compare the SHG efficiency for the three resonances in this configuration and in the stationary regime. We found that the efficiency associated with the second resonance is 43 times larger than the efficiency associated with the first and 100 times the efficiency associated with the third. In the following, we compare SHG efficiencies in the stationary regime in order to avoid the effects associated with spectral filtering and group velocity mismatch.

A crucial point to be considered is the evolution of the SHG intensity as a function of the number of unit cells of the NL 1D-PC WG. In a planar structure where losses can be neglected, the conjugated effect of phase matching and enhancement of DOMs leads to a second-harmonic efficiency growth that follows the sixth power of the structure length, far better than the usual quadratic behavior associated with second-order nonlinear effects. In Fig. 8 is represented on a logarithmic scale the SHG efficiency η as a function of the number of unit cells N, for the optimized $h=2\ \mu$m (circles) and the nonoptimized $h=1\ \mu$m (squares) structures. The FF

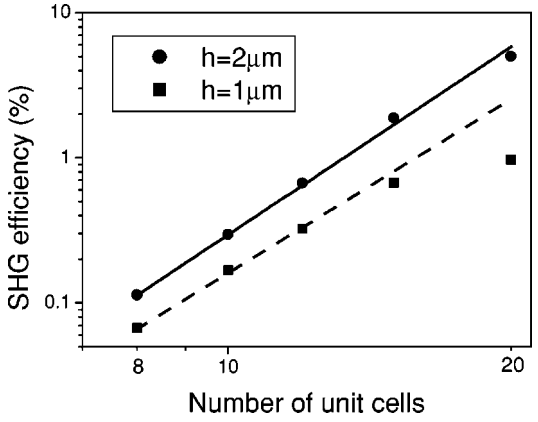

FIG. 8. SH conversion efficiency versus the number of periods N of the structure on a logarithmic scale. The SHG efficiencies of the $h=1$ and the 2 μm structures are represented, respectively, by squares and circles. The linear fit of these efficiencies is also plotted as the dashed line for the $h=1$ μm and as the solid line for the $h=2$ μm structures.

peak power is 600 W, the mode extension in the z direction is 5 μm. The best linear fit of the dots is given by the full line. One should stress that this result does not mean that N could be increased arbitrarily keeping the same slope for the conversion efficiency. Indeed, as the number of periods increases, the lifetime of photons in the PBG structure at SH wavelength increases as well and the effect of losses will become predominant. This is already the case for the nonoptimized sample.

IV. ANALYTICAL EQUIVALENT-CAVITY MODEL AND DISCUSSION

In the previous sections we have shown how numerical simulation, via FDTD, of the nonlinear properties of the periodic waveguide is able to give precise information on the role played by losses in the SHG efficiency. Time consumption makes the implementation of such numerical codes unsuitable when the number of periods is further increased to $N=30$ or more. In order to better understand the meaning of the numerical results obtained as well as to use them to predict the SHG efficiency as the number of periods is further increased, we will introduce in this section a phenomenological approach that considers the periodical waveguide as a longitudinal cavity. This cavity represents the distributed resonator, doubly resonant at the FF and the SH. We will refer to this approach as the equivalent-cavity model. The internal SHG efficiency η_{int} in an equivalent cavity depends on the accumulated fields at FF frequency [17]:

$$\eta_{\mathrm{int}} \propto (\rho^{\omega} \times L)^2, \tag{2}$$

where $\rho^{\omega,2\omega}=1/\nu_g^{\omega,2\omega}$ is the normalized density of optical modes [13] at the FF,SH frequencies and $\nu_g^{\omega,2\omega}$ is the group velocity. Calling $L=N\Lambda$ the total length, one can rewrite the conversion efficiency in terms of the equivalent-cavity lifetime at FF,SH frequencies $\tau^{\omega,2\omega}$:

$$\eta_{\mathrm{int}} \propto \left(\frac{L}{\nu_g^{\omega}}\right)^2 = (\tau^{\omega})^2. \tag{3}$$

The cavity lifetime $\tau^{\omega,2\omega}$ can be written as

$$\frac{1}{\tau^{\omega,2\omega}} = \frac{1}{\tau_L^{\omega,2\omega}} + \frac{1}{\tau_R^{\omega,2\omega}}, \tag{4}$$

where $\tau_L^{\omega,2\omega}$ is the longitudinal escape time and $\tau_R^{\omega,2\omega}$ the coupling time with radiative modes. The latter is associated with the losses at FF,SH frequencies. Using the preceding definitions the SHG efficiency is written as

$$\eta_{\mathrm{int}} \propto \left(\frac{\tau_L^{\omega}\tau_R^{\omega}}{\tau_R^{\omega}+\tau_L^{\omega}}\right)^2. \tag{5}$$

The last equation is relevant for the internal SHG. However, as we detect only the guided part of the second-harmonic signal, the effective efficiency is given by

$$\eta_{\mathrm{eff}} = \eta_{\mathrm{int}} \frac{\tau_R^{2\omega}}{\tau_R^{2\omega}+\tau_L^{2\omega}} \propto \left(\frac{\tau_L^{\omega}\tau_R^{\omega}}{\tau_R^{\omega}+\tau_L^{\omega}}\right)^2 \frac{\tau_R^{2\omega}}{\tau_R^{2\omega}+\tau_L^{2\omega}}. \tag{6}$$

From Ref. [13], for a lateral resonance in a multilayer structure, we have the relation $\rho^{\omega,2\omega} \propto N^2$, which implies $\tau_L^{\omega,2\omega} \propto N^3$. Note that $\tau_R^{\omega,2\omega}$ is to some extent independent of the number of periods. Then, depending on the relative values of different relevant times, three asymptotic regimes can be identified:

(1) Negligible losses at both the FF and SH: $\tau_L^{\omega} \ll \tau_R^{\omega}$ and $\tau_L^{2\omega} \ll \tau_R^{2\omega}$,

$$\eta_{\mathrm{eff}} \propto (\tau_L^{\omega})^2 \propto N^6.$$

(2) Negligible losses only at the FF: $\tau_L^{\omega} \ll \tau_R^{\omega}$ and $\tau_L^{2\omega} \gg \tau_R^{2\omega}$,

$$\eta_{\mathrm{eff}} \propto \frac{(\tau_L^{\omega})^2}{\tau_L^{2\omega}} \propto N^3.$$

(3) Losses at the FF and SH: $\tau_L^{\omega} \gg \tau_R^{\omega}$ and $\tau_L^{2\omega} \gg \tau_R^{2\omega}$,

$$\eta_{\mathrm{eff}} \propto \frac{1}{\tau_L^{2\omega}} \propto \frac{1}{N^3}.$$

In this equivalent-cavity model, the ratio $\tau_R^{\omega,2\omega}/(\tau_R^{\omega,2\omega}+\tau_L^{\omega,2\omega})$ can be related to the transmission coefficients $T^{\omega,2\omega}$ at resonances:

$$T^{\omega,2\omega} = \left(\frac{1}{1+\tau_L^{\omega,2\omega}/\tau_R^{\omega,2\omega}}\right) = \left(\frac{1}{1+N^3/k^{\omega,2\omega}}\right), \tag{7}$$

where $k^{\omega,2\omega}$ is a constant.

We applied this model to the waveguide ($h=1$ and 2 μm) studied numerically in the previous section. Using the results of the linear FDTD code one can numerically obtain the transmission coefficients at FF and SH frequencies. They are reported in Table I. For the deep etched waveguide T^{ω} is close to unity over the whole range of the number of periods

TABLE I. Value of the linear transmission for the first guided mode at FF and SH frequencies. $k^{\omega,2\omega}$ are inferred using Eq. (7) and numerical data.

	$h=1\ \mu$m		$h=2\ \mu$m
N	T^{ω}	$T^{2\omega}$	$T^{2\omega}$
8	0.95	0.76	0.95
10	0.93	0.74	0.91
12	0.89	0.62	0.85
15	0.83	0.50	0.81
20	0.71	0.20	0.65
	$k^{\omega}=15\,194$	$k^{2\omega}=2668$	$k^{2\omega}=13\,685$

explored. This means that, in this case, losses can be neglected and $\tau_R^{\omega}\rightarrow\infty$. For the other situations, the constant $k^{\omega,2\omega}$, defined in Eq. (7), can be inferred from a fit of numerical values obtained for the transmission coefficients. The results of the fit are also presented in Table I. The effective SHG efficiency can now be expressed as

$$\eta_{\text{eff}}\propto N^6\left(\frac{1}{1+N^3/k^{\omega}}\right)^2\left(\frac{1}{1+N^3/k^{2\omega}}\right). \tag{8}$$

At this point, using only linear simulations, we know the exact dependence of the SHG on the length structure. The only unknown parameter is the exact amplitude of η_{eff}, which is determined by fitting the numerically calculated SHG efficiency.

The results obtained for the $h=1\ \mu$m and the $h=2\ \mu$m waveguides are represented by full lines in Figs. 9(a) and 9(b), respectively. Squares represent the NL FDTD results. The N^6 asymptotic law and the usual quadratic law are also represented in dotted and dashed lines, respectively. The equivalent-cavity model clearly shows that for $N>20$ the SHG efficiency of $h=1\ \mu$m waveguide saturates and decreases below the N^2 law, illustrating the regime where losses in the FF and SH cannot be neglected. Conversely, the $h=2\ \mu$m waveguide SHG efficiency increases with a slope close to the N^6 law, illustrating the situation where losses in the FF are negligible where those in the SH start to play a role.

Finally, two important points concerning the validity of the analytical approach should be stressed. (1) As is the case in the NL FDTD numerical approach, the FF depletion is neglected in the equivalent-cavity model. This limits the validity of the model to efficiencies below 15%. (2) For the $h=2\ \mu$m structure losses were neglected at the FF frequency; as the number of periods is increased, such losses will become measurable and can no longer be neglected. Nevertheless, it is reasonable to consider that, taking into account the preceding restrictions, analytical results give a good estimate of the conversion efficiency. In particular, a SHG conversion efficiency of the order of 15% is predicted, with a FF power of 600 W for structures of $N<30$ corresponding to a maximal total length of 7.5 μm.

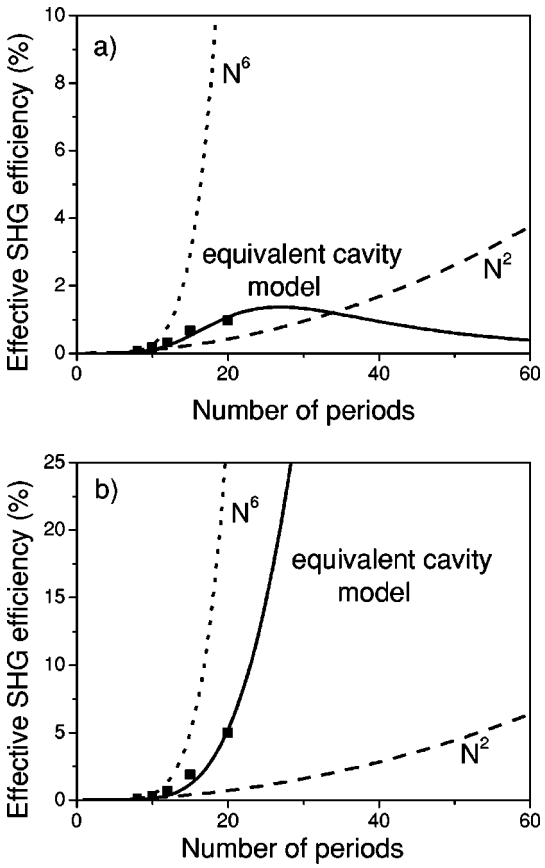

FIG. 9. Conversion efficiency predicted by the equivalent-cavity model (full line) and the NL FDTD code (squares). The asymptotic N^6 law and the usual quadratic law are represented (dotted and dashed lines, respectively). (a) and (b) correspond to the $h=1$ and 2 μm structures, respectively.

V. CONCLUSION

In conclusion we propose and optimize a 1D-periodic photonic edge dual wavelength WG operating as an efficient SH generator. We analyze the role of structure parameters and diffractive losses in such a waveguide using a NL 2D FDTD code. A SHG efficiency of 5%, for 600 W FF peak power, is predicted in a technologically realistic semiconductor 20-period, 5-μm-long structure. A phenomenological model is proposed in order to evaluate the conversion efficiency as the number of periods is further increased. It is shown that if the losses at FF frequency are negligible the conversion efficiency can be further improved by a sizable amount. The model provides a simple tool to extrapolate the results obtained with the numerical code to a number of periods for which time consumption makes FDTD not suitable.

ACKNOWLEDGMENT

This work was supported by Action Concertée Nanosciences "CPNonlin."

[1] N. Bloembergen and J. Sievers, Appl. Phys. Lett. **17**, 483 (1970).
[2] J. P. van der Ziel, Appl. Phys. Lett. **28**, 437 (1976).
[3] M. Scalora, M. J. Bloemer, A. S. Manka, J. P. Dowling, C. M. Bowden, R. Wiswanathan, and J. W. Haus, Phys. Rev. A **56**, 3166 (1997).
[4] M. Centini, C. Sibilia, M. Scalora, G. D'Aguanno, M. Bertolotti, M. J. Bloemer, C. M. Bowden, and I. Nefedov, Phys. Rev. E **60**, 4891 (1999).
[5] T. F. Krauss, R. M. De La Rue, and S. Brand, Nature (London) **383**, 699 (1996).
[6] Y. Dumeige, I. Sagnes, P. Monnier, P. Vidakovic, I. Abram, C. Mériadec, and A. Levenson, Phys. Rev. Lett. **89**, 043901 (2002).
[7] C. De Angelis, F. Gringoli, M. Midrio, D. Modotto, J. S. Aitchison, and G. F. Nalesso, J. Opt. Soc. Am. B **18**, 348 (2001).
[8] A. Fiore, V. Berger, E. Rosencher, P. Bravetti, and J. Nagle, Nature (London) **391**, 463 (1998).
[9] V. Berger, I. Pavel, E. Ducloux, and F. Lafon, J. Appl. Phys. **82**, 5300 (1997); M. Palamaru and Ph. Lalanne, Appl. Phys. Lett. **78**, 1466 (2001).
[10] D. Pezzetta, C. Sibilia, M. Bertolotti, J. W. Haus, M. Scalora, M. J. Bloemer, and C. M. Bowden, J. Opt. Soc. Am. B **18**, 1326 (2001); M. Midrio, L. Socci, and M. Romagnoli, *ibid.* **19**, 83 (2002); D. Pezzetta, C. Sibilia, M. Bertolotti, R. Ramponi, R. Osellame, M. Marangoni, J. W. Haus, M. Scalora, M. J. Bloemer, and C. M. Bowden, *ibid.* **19**, 2102 (2002).
[11] P. Lalanne, IEEE J. Quantum Electron. **38**, 800 (2002).
[12] A. Taflove, *Computational Electrodynamics: The Finite Difference Time Domain Method* (Hartech, Boston, MA, 1995).
[13] J. M. Bendickson, J. P. Dowling, and M. Scalora, Phys. Rev. E **53**, 4107 (1996); J. P. Dowling, M. Scalora, M. J. Bloemer, and C. M. Bowden, J. Appl. Phys. **75**, 1896 (1994).
[14] B. Shi, Z. M. Jiang, X. F. Zhou, and X. Wang, J. Appl. Phys. **91**, 6769 (2002).
[15] F. Raineri, Y. Dumeige, J. A. Levenson, and X. Letartre, Electron. Lett. **38**, 1704 (2002).
[16] A. M. Zhleltikov, A. V. Tarasishin, and S. A. Magnitskii, JETP Lett. **91**, 298 (2000).
[17] G. D'Aguanno, M. Centini, M. Scalora, C. Sibilia, Y. Dumeige, P. Vidakovic, J. A. Levenson, M. J. Bloemer, C. M. Bowden, J. W. Haus, and M. Bertolotti, Phys. Rev. E **64**, 016609 (2001).